Computer Microvision for MEMS

Academic and Research Staff
Professor Dennis M. Freeman, Professor Berthold K. P. Horn, Michael B. McIlrath

Graduate Students
Salil P. Desai, Stanley S. Hong, Jekwan Ryu

Support Staff
Janice Balzer

1. Computer Microvision for MEMS

Sponsors
Defense Advanced Research Projects Agency, Grant F30602-97-2-0106
Center for National Research Initiatives, Matisse Project

Project Staff
Professor Dennis M. Freeman, Michael B. McIlrath, Salil P. Desai

Collaborators
Carnegie Mellon University
Sarnoff Corporation
University of California at Berkeley
University of Southern California Information Sciences Institute

Introduction

Computer Microvision is a tool for in situ visualization of the motions of internal structures in microelectromechanical systems (MEMS), that operates by combining light microscopy, video imaging, and machine vision. Images of MEMS are magnified with a microscope and projected onto a digital CCD camera. Stroboscopic illumination is used to take temporal sequences of images at multiple planes of focus. Recorded images are then viewed at playback speeds chosen to facilitate human interpretation of the motions. Quantitative estimates of motions are also obtained directly from the recorded images using algorithms originally conceived for robot vision.

Complete Computer Microvision systems have been installed and are in active use at Carnegie Mellon University (CMU), University of California at Berkeley Sensors and Actuators Center (BSAC), and the MIT Gas Turbine Laboratory. These Computer Microvision test stations each consist of a Zeiss Axioplan 2 laboratory microscope equipped with long working distance objectives. The microscope stages are equipped for remote control of 3D position via an integral motorized Z drive and a Prior Scientific 4" x 3" motorized X-Y stage. A piezoelectric objective nanopositioner provides precise control of axial position. A megapixel CCD camera connects to a Pentium-based computer running the Linux kernel via a Coreco digital frame grabber.

A number of improvements were made to the Computer Microvision hardware. Electrical stimulation of the device under test, stroboscopic illumination, and exposure control of the camera are accomplished by a single custom hardware stimulus and illumination control module (SICM) subsystem. The SICM logic is entirely implemented by downloadable firmware and is under operational control of the Computer Microvision system data acquisition software at runtime. The SICM firmware was enchanced for more precise, flexible, and efficient control across a wider range of stimulus and measurement conditions. The new implementation provides up to 65,536 phase divisions per stimulus period. Exposure times requiring a non-integer number of phases to be strobed are now accurate and precise. Host computer communications and host software camera integration control were made substantially more robust. The SICM was modified to provide the MEMS with a stimulus signal of up to ±10 volts.

The Computer Microvision system software architecture was implemented to achieve highly flexible run-time configurability and the separation of operational functionality from user interface. The independence of functionality from user interface enabled us to build and experiment with a variety of user interfaces, GUI technologies, and client platforms for remote operation without changing the service implementation. The software architecture also supports local and remote service invocation using various protocols such as HTTP and XML-RPC. Run-time selectable and dynamically loadable software modules implement most core functionality of the data acquisition system.

For use on the SuperNet, a wide-area, advanced networking testbed supported by the DARPA NGI (Next Generation Internet) program, we developed a data storage module which saves image frame data to the Distributed Parallel Storage System (DPSS) developed by Lawrence Berkeley Laboratories (LBL). We installed a DPSS server installation locally for testing and demonstrated image storage and retrieval over SuperNet using DPSS installations at LBL and the University of Southern California Information Sciences Institute (ISI). This storage module was installed and is selectable at run-time at the other SuperNet-enabled Computer Microvision sites at BSAC and CMU. We also developed a multi streamed video service with adaptable buffering for real-time focus and live stroboscopic motion display over the SuperNet and other high bandwidth networks.

Additionally, we added support for the Coreco PC-DIG PCI bus framegrabber to the Computer Microvision system. This is a single board digital camera interface card that can handle pixel data rates up to 40 megahertz.

We added several additional capabilities to the motion analysis software. The architecture of the analysis programs was modified to enable easy "drop in" of user-written motion analysis code. Such codes can be specified and linked at run time from a shareable dynamically loadable object file, rather than having to be bound into a static executable image. In this new framework, a more sophisticated motion analysis algorithm package has been developed. This implementation includes independent features which can be specified or controlled at run time: linear bias correction (LBC) can optionally be applied to the computed displacement estimate to improve its accuracy, and singular value decomposition (SVD) can be used to improve the robustness of the estimate.

In collaboration with researchers at CNRI and UCB, we designed an extensible markup language (XML) dataset document type definition for describing Microvision and other Matisse project experiments. The document type definition (DTD) includes specification of experimental setup and parameters, data type and geometry, test signal characteristics, and experiment identification and comments. A configuration property list element supports the recording of open-ended application configuration information without requiring modification of the DTD itself. For maximal extensibility, the DTD itself is stored at the beginning of each such XML experimental dataset descriptor. An XML document is associated and stored with each recorded experimental dataset, and includes a reference to the binary image datafile. The XML dataset descriptor was designed to be used for information storage and retrieval, playback, analysis, and user interface presentation control. These capabilities were demonstrated in conjunction with software infrastructure developed by Sarnoff Corporation.

We worked with users of the Computer Microvision systems at Berkeley, CMU, and MIT to resolve problems and provide support on various system issues, including measurement throughput, host resource consumption, output presentation capabilities, supernet access, installation on multiple distribution platforms, and security, among others. Some of these areas have been addressed more completely in updated versions of the Computer Microvision system.

In conjunction with ISI, we designed and implemented the switching and addressing architecture for our interconnect to the SuperNet. A local optical fiber loop carries both MIT net and SuperNet traffic, so end stations on the fiber (e.g., Computer Microvision systems) can have both Internet

and SuperNet addresses without requiring multiple network interface cards (NICs). The SuperNet gigabit feed is isolated in a virtual LAN (VLAN) configuration at our laboratory core router. An ATM link operates on a separate wavelength; this path can be available if necessary for redundancy or backup. We have also added gigabit switches and Supernet routing to our local segment of the MIT network, enabling gigabit over copper access to end stations not on the optical fiber. Routing information is exchanged with Collaborative Advanced Internet Research Network (CAIRN) routers, providing end stations with dynamically updated SuperNet routing information, while allowing transparent Internet and MIT local net connectivity.

Experiment to CAD Model collaborations with Carnegie Mellon University

In collaboration with researchers at CMU, experimental results (using conventional brightfield and interferometric images) for a folded flexure lateral resonator (Figure 1) designed at MIT and fabricated using the Cronos MUMPS process were compared to simulations with NODAS (Nodal Design of Actuators and Sensors), a system-level simulation tool developed at CMU and based on Cadence design tools and Verilog-A. Model parameters were determined directly from layout and MUMPS processing results. Measurements were made of motion in six degrees of freedom. For the folded flexure resonator the dominant modes of motion are translation in y, translation in z and rotation about x. CMU and MIT researchers worked together to verify the Verilog-A simulation with measurements taken with the Computer Microvision system. The NODAS simulated resonant frequencies matched measured resonant frequencies to within 5% to 10%, as shown in Figures 2, 3, and 4.

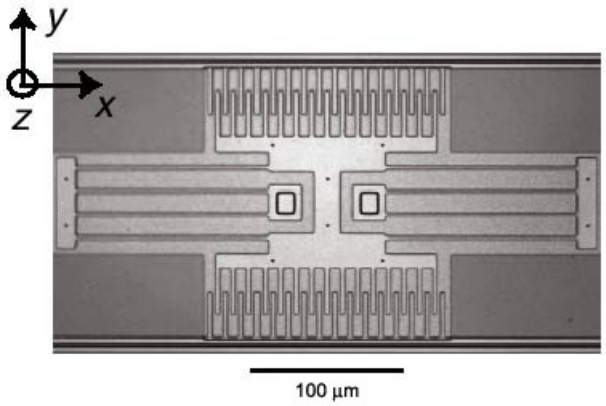

Figure 1: Optical micrograph of polysilicon surface micromachined lateral resonator fabricated using Cronos MUMPs fabrication process.

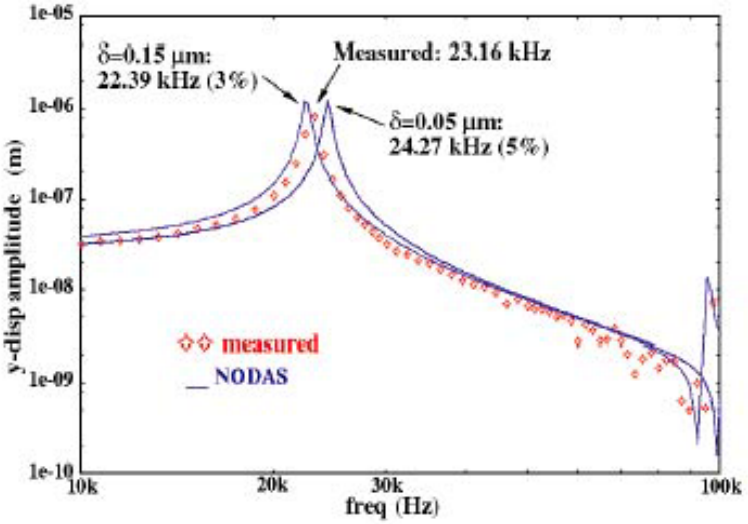

Figure 2: Comparison of Computer Microvision measurements (dotted line) and simulations (solid line) of frequency response in the y-direction.

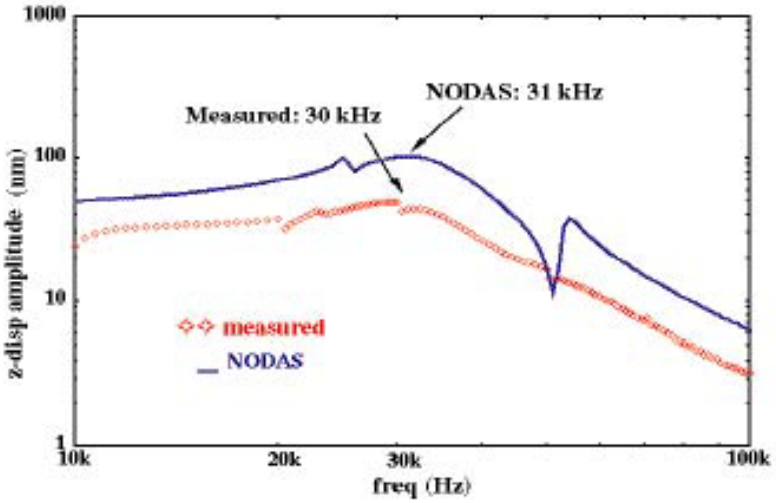

Figure 3: Comparison of Computer Microvision measurements (dotted line) and simulations (solid line) of frequency response in the z-direction.

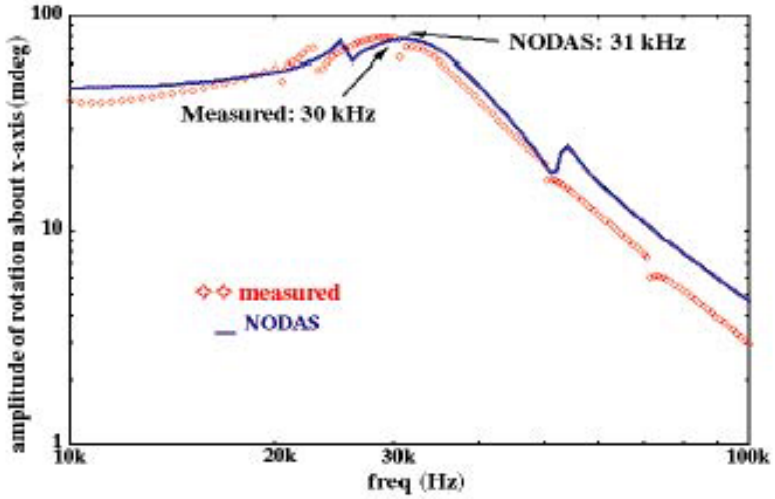

Figure 4: Comparison of Computer Microvision measurements (dotted line) and simulations (solid line) of frequency response for rotation about the x-direction.

Conventional polysilicon-based surface micromachining processes, such as Sandia SUMMiT IV and Cronos MUMPs, offer several polysilicon structural layers for designing increasingly complex microstructures. However, since all the structural layers are electrically conducting, there is no effective means of routing different electrical signals through a single structural layer. Hence, designing devices with multiple degrees of freedom in a polysilicon based surface micromachining process is difficult. The CMU CMOS MEMS process is ideal for designing devices with multiple degrees of freedom. The key feature of this CMOS MEMS process technology is the ability to make composite metal/insulator microstructures with very narrow beam widths and air gaps, enabling electrostatic actuation with a wide range of electromechanical design possibilities. The CMOS metallization and dielectric layers, normally used for electrical interconnect, serve a dual function as structural layers. Each structural element can consist of as many as 3 electrically isolated metal layers (referred to as metal-1, metal-2 and metal-3). This allows for considerable design flexibility in electrical routing.

A multiple degree-of-freedom test structure was designed and fabricated using the CMU CMOS MEMS process (as part of the DARPA MEMS sponsored Application Specific Integrated MEMS Process Service). The CMOS fabrication was performed at Austria Mikro Systeme and the post-CMOS micromachining at the CMU MEMS Laboratory. This test structure is an integral part of a measurement and modeling collaboration with the CMU MEMS Laboratory. The goal of the collaborative project is to compare Mirau interferometric Computer Microvision measurements of the device with simulation results obtained from NODAS software.

The multiple degree-of-freedom test structure is essentially a comb-drive lateral resonator (Figure 5). The resonator is anchored to a frame, which provides first order curl-matching (Figure 6). The curl-matching frame is, in turn, anchored to the surrounding metal-3 layer.

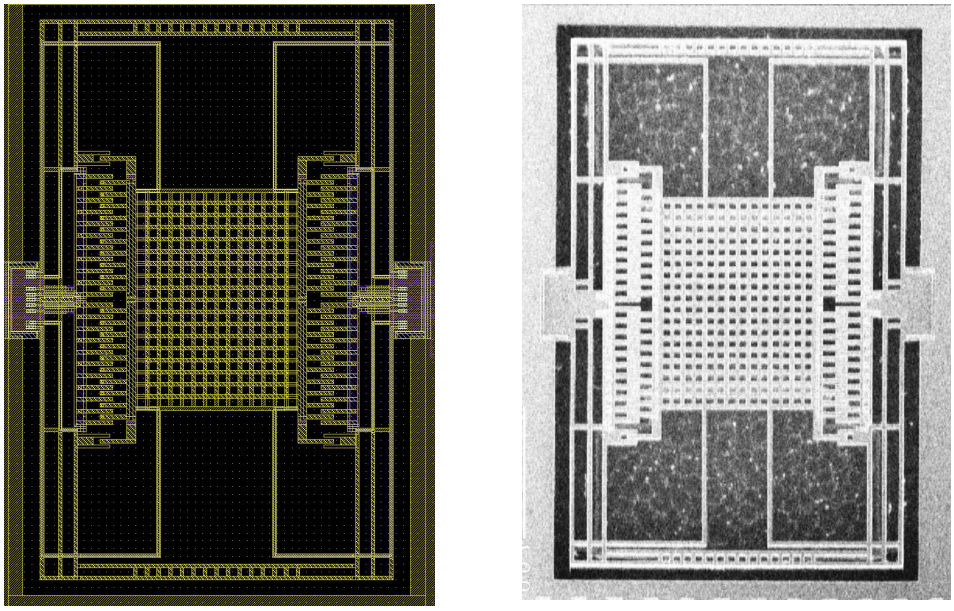

Figure 5: Six Degree-of-Freedom Test Structure. The left panel shows the layout of the structure that we designed. The structure was fabricated using CMU's CMOS MEMS process. The right panel shows an Scanning Electron Micrograph (SEM) of the resulting structure.

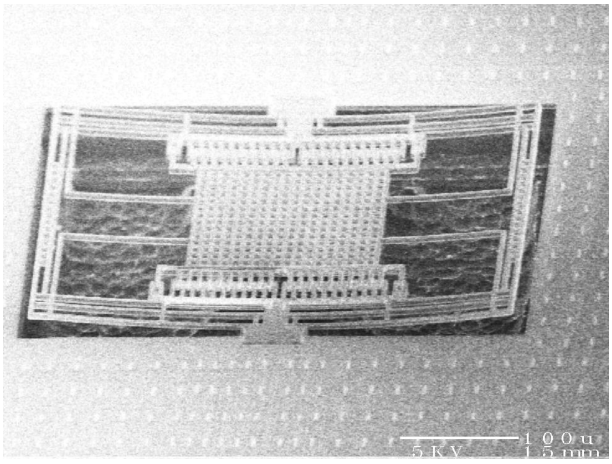

Figure 6: Oblique View of Six Degree-of-Freedom Test Structure. This SEM illustrates the first-order curl matching achieved in our test structure. The curl of the frame that surrounds the resonator nearly matches that of the resonator.

The rotor and stator comb fingers are divided into two electrically isolated arrays. On the stator comb drive, the metal layers in each array are routed to separate bond pads. On the rotor array, the metal-2 and metal-3 layers in each comb-finger array are shorted. Electrical connections to the rotor combs are made by routing metal lines through the curl-matching frame and the flexures. Limit-stops are placed at each end of the comb drives to limit motions of the proof mass and prevent shorting of the device (Figure 7).

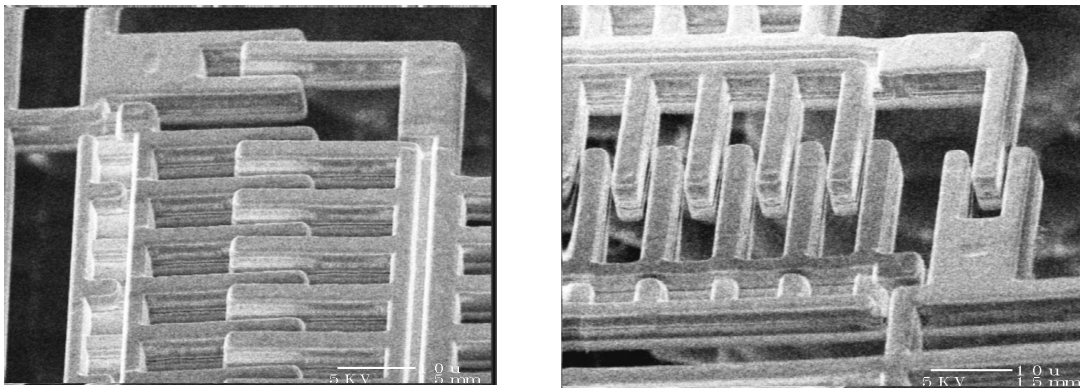

Figure 7: Interdigitated Teeth of Six Degree-of-Freedom Test Structure. These SEMs show views of teeth in the opposing comb drives that attach to the resonator and frame, respectively.

The proof mass consists of all 3 metal layers, which are electrically shorted. The device can be actuated in multiple degrees of freedom, since different voltage signals can be applied to each metal layer in the stator comb-finger arrays. Two designs of the test structure, with different flexure dimensions, were included in the final design. In addition to these devices, folded flexure resonators and crab-leg flexure resonators (Figure 8) both designed at CMU, were included on the chip.

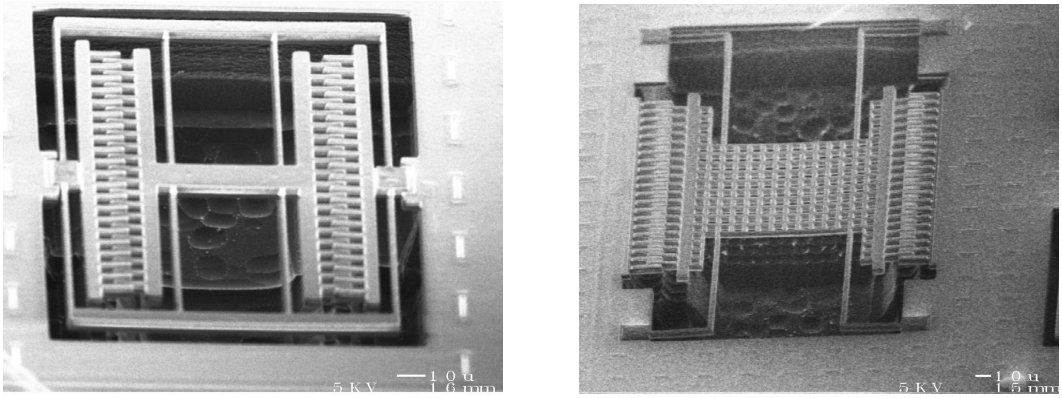

Figure 8: Folded Flexure and Crab-Leg Flexure Resonators. These designs provided by CMU were also incorporated on our test chip.

Our goal is to measure important geometrical parameters such as feature dimensions and thicknesses of air gaps using Computer Microvision techniques. Based on those parameters, NODAS will be used to simulate motions that will be compared with measurements by Computer Microvision. The long term goal is to close the design/simulate/measure loop to improve simulation tools for MEMS.

Publications

Theses

S.P. Desai, *Mirau Interferometric Computer Microvision*, S.M. thesis, Department of Electrical Engineering and Computer Science, MIT, 2002.

2. Synthetic Aperture Lithography

Sponsor
Defense Advanced Research Projects Agency, Grant N66001-00-1-8908

Project Staff
Professor Dennis M. Freeman, Professor Berthold K. P. Horn, Stanley S. Hong, Jekwan Ryu

Collaborator
Lightwave Instruments, LLC

Introduction
We have developed a novel approach to lensless and maskless projection of arbitrary optical patterns, which we call Synthetic Aperture Lithography (SAL). In traditional optical lithography, light from an illuminator passes through a mask and is focused by a lens to recreate the mask pattern on a wafer. The central idea in SAL is that the pattern of light that emerges from a lens will evolve into the same lithographic pattern regardless of how it was created. SAL replaces the lens, the mask, and the mask illuminator with a discrete set of controllable laser beams. By controlling the amplitudes and phases of the beams, lithographic patterns with diffraction-limited lateral resolution and essentially unlimited depth of focus can be projected. To explore the scalability of the SAL concept to short wavelengths, we constructed all-reflective SAL pattern projector.

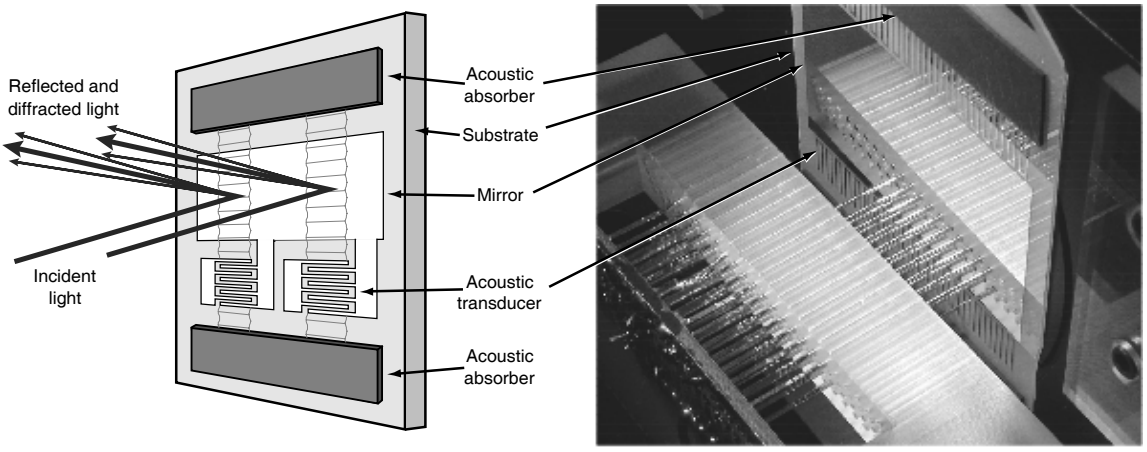

Figure 1: The left panel shows an illustration of a surface acoustic wave optical modulator (SAW-Mod). Only two channels are shown for clarity. The right panel shows a photograph of a SAW-Mod prototype. The reflection of a spring contact probe array is seen in the mirror.

Surface Acoustic Wave Optical Modulator

A reflective optical modulator was developed using surface acoustic waves (Figure 1). Surface acoustic waves (SAWs) are generated using interdigital transducers (IDTs, 30 finger pairs, resonant frequency 50 MHz, 700 mm acoustic aperture) microfabricated on a piezoelectric substrate (SAW grade lithium niobate, Y-cut, Z-propagating). The RF input impedance of each IDT is matched to the output impedance of an RF amplifier using a two element impedance matching circuit (VSWR < 1.3). Each bidirectional IDT generates a forward-propagating SAW that deforms the surface of a common mirror and an unused backward-propagating SAW.

(Acoustic absorbers dissipate the SAWs and prevent the formation of standing waves.) Light incident on the mirror is diffracted by the surface deformations (or ripples) caused by the SAWs.

Figure 2 shows the diffracted field produced by an eight channel SAW optical modulator (SAW-Mod) when the cylindrically expanded beam of an argon ion laser (λ = 488 nm) is incident on the mirror approximately 1 cm from the top edge of the IDTs. Because the SAWs are laterally well-confined (essentially acoustic beams), only the vertical strips of mirror directly above each IDT are deformed; the outputs of individual channels are resolved. The first order diffraction efficiency of the SAW-Mod is shown in Figure 3. With an input RF power of 5.0 W at 50 MHz, the measured first order diffraction efficiencies are 6.0%, 1.4%, and 0.82% at optical wavelengths of 244 nm, 488 nm, and 633 nm, respectively. These results are in agreement with theory. Figure 4 shows an optical signal to crosstalk ratio of 17 dB between adjacent SAW-Mod channels. Figure 5 shows the optical rise time of the SAW-Mod. The measured 820 ns rise time is principally determined by the length of the IDT.

Modulation of optical phase is demonstrated in Figure 6, where the optical phase difference between two +1 order diffracted beams produced by two SAW-Mod channels was detected by overlapping the two beams onto a CCD and imaging the resulting interference fringes. The two channels were driven at the same amplitude and frequency. As shown, the spatial phase of the fringe pattern (which is determined by the optical phase difference between the diffracted beams) shifts in response to the RF phase difference between the signals driving the two channels. The visibility of the fringe patterns suggests that the frequencies of the diffracted beams were shifted by the same amount (the CCD integration time was several ms).

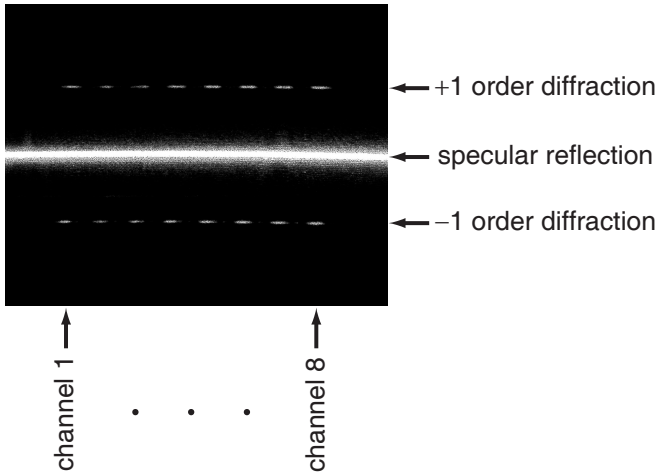

Figure 2: Diffracted field generated by an eight channel SAW-Mod. Eight +1 order diffracted beams, eight -1 order diffracted beams, and the specular reflection of a cylindrically expanded incident laser beam are visible.

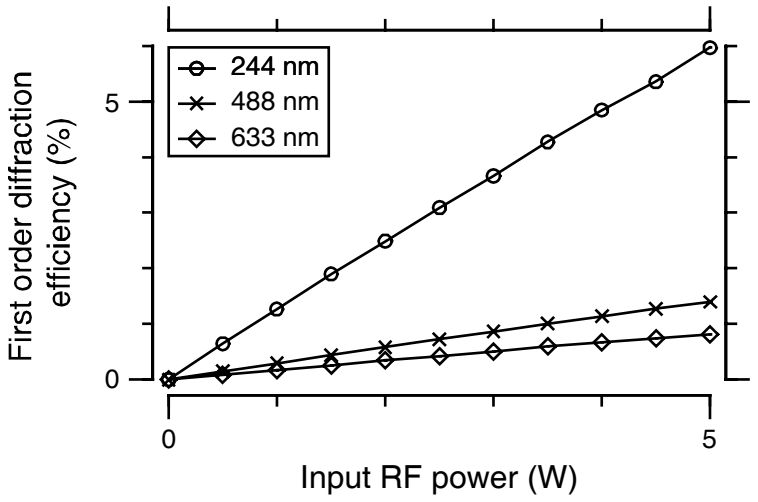

Figure 3: First order diffraction efficiency versus input RF power for a single SAW-Mod channel.

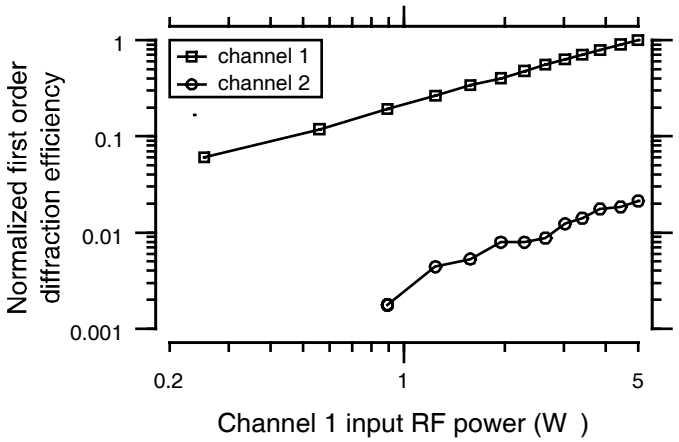

Figure 4: Crosstalk between two adjacent SAW-Mod channels. The input to channel 1 was varied while the input to channel 2 was turned off.

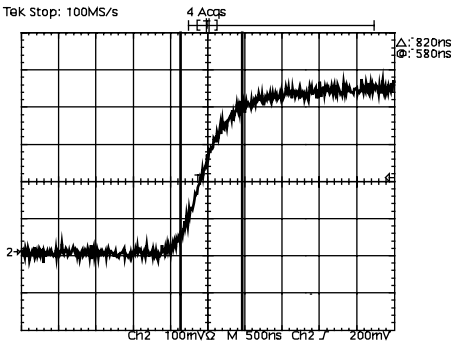

Figure 5: Optical rise time of a single SAW-Mod channel. The amplified output of a high-speed photodiode is shown in response to a step input to the SAW-Mod.

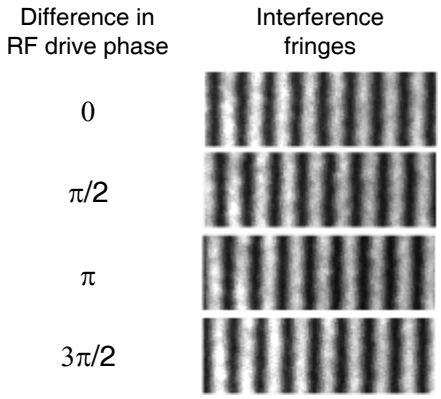

Figure 6: Modulation of optical phase. Optical phase was detected by interfering two +1 order diffracted beams generated by two SAW-Mod channels. The spatial phase of the resulting fringe pattern shifts in response to the RF phase difference between the drive signals.

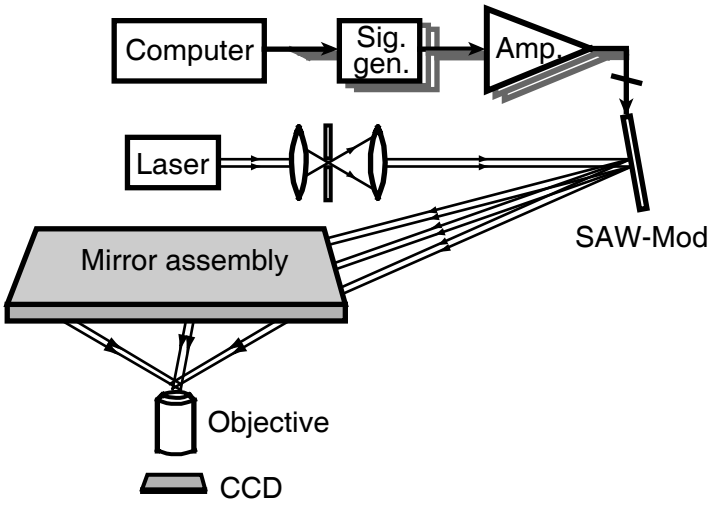

Figure 7: Schematic diagram of the all-reflective SAL pattern projector. Only 3 beams are shown for clarity.

Needle of Light

Figure 7 shows the all-reflective SAL pattern projector schematically. The beam of a single line (λ = 488 nm) argon ion laser was spatially filtered, expanded, and then split into 15 diffracted beams using a 15 channel SAW-Mod. The 15 beams were then steered by an array of mirrors so that the beams approached the target region on the surface of an imaginary cone with a half angle of 72 degrees (0.95 NA). The 15 beams were linearly polarized perpendicular to the central axis of the cone (TE or S polarization). The working distance of the projector was more than 2.8 cm. The light pattern generated by the interference of the 15 beams was projected into the oil-immersed focal plane of a 160x /1.4 NA microscope objective and sampled with a CCD imager.

For mechanical stability, the mirror assembly was constructed on a single thick plate of aluminum. Mirror locations were numerically optimized to minimize path length differences across beams. Although it was necessary to match the path lengths to within the coherence length of the laser, it was neither necessary nor desired to match the path lengths with sub-wavelength precision. The amplitudes and phases of the beams at the point of interference were estimated from images of interference patterns captured by the CCD imager using an iterative algorithm. Sub-wavelength optical alignment was achieved by dividing and subtracting the measured beam amplitudes and phases from the commanded SAW-Mod amplitudes and phases, respectively.

The amplitudes and phases of the beams were adjusted to constructively interfere at the the center pixel of the CCD imager. The resulting pattern of light is shown in Figure 8. Notice that there is a single bright dot near the center of the measured image surrounded by background clutter. The diameter of the dot (FWHM) is less than 0.44 λ. The clutter can be attributed to the finite number of beams. As the number of beams in increased in simulation, the clutter moves away from the dot and the pattern approaches a nondiffracting Bessel beam. The length of the needle was experimentally determined by translating the microscope objective with a piezoelectric nanopositioner. A sequence of 101 images at planes separated by 1 mm was assembled into a 3D image. Figure 8 shows three representative planes along with an axial cut through the center. The cut illustrates a depth of focus of more than 100 λ.

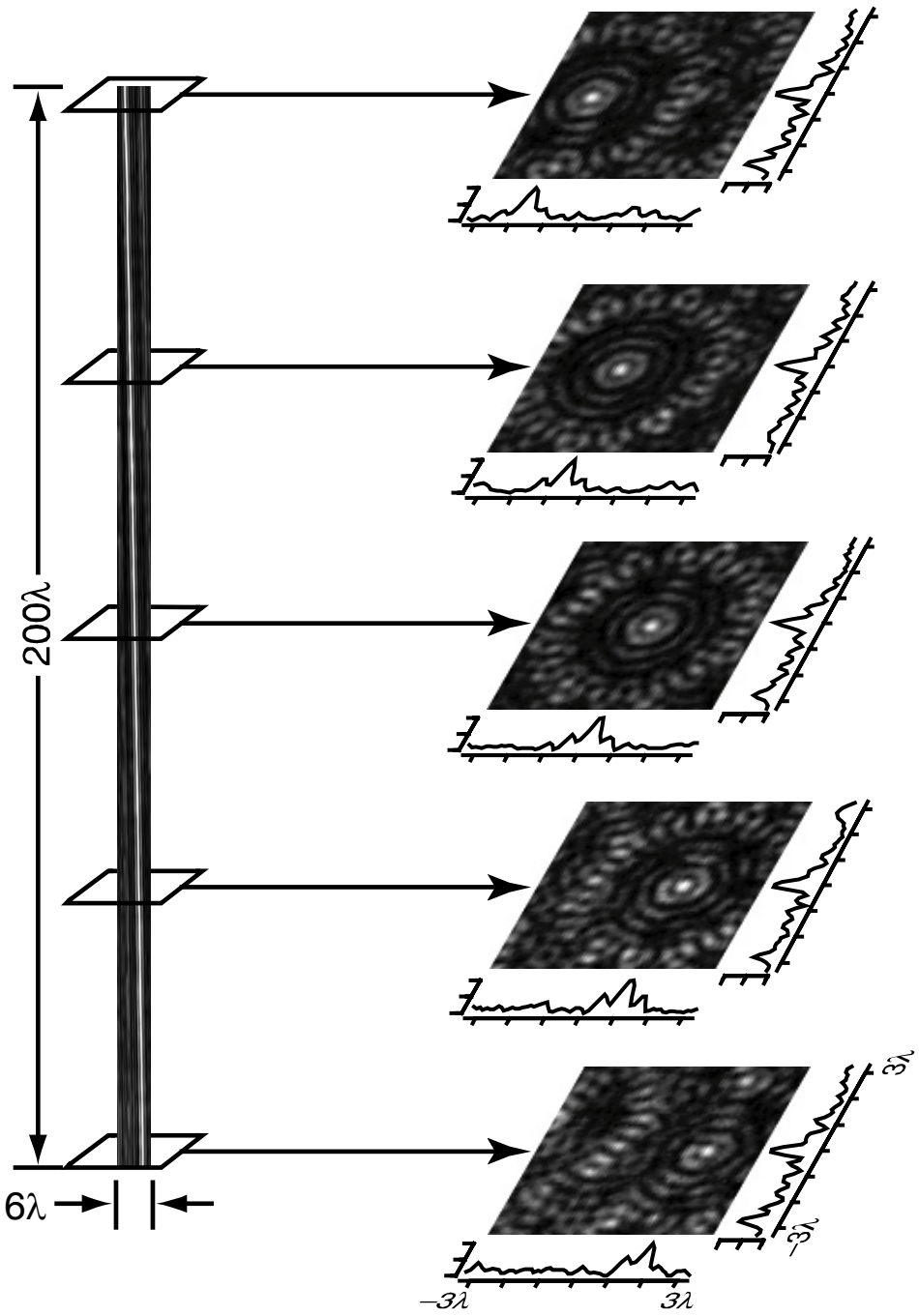

Figure 8: Measured needle of light produced with a 15 beam 0.95 NA all-reflective SAL pattern projector. The right panels show images at 5 planes of focus separated by 25 mm. The center row of pixels from a series of 101 similar images are stacked to form the left image, which illustrates the axial structure of the pattern. The needle of light is less than 0.44 λ in diameter (FWHM) and over 100 λ in length.

Conference Presentations

M.S. Mermelstein, S.S. Hong, J. Ryu, D.M. Freeman, "Synthetic Aperture Lithography," invited talk, *2002 International Conference on Electron, Ion and Photon Beam Technology and Nanofabrication*, Anaheim, California, May 28-31, 2002.

Journal Articles, Submitted for Publication

M.S. Mermelstein, S.S. Hong, J. Ryu, D.M. Freeman, "Interfering multiple electronically controlled beams to produce a needle of light," submitted to the *2002 International Conference on Electron, Ion and Photon Beam Technology and Nanofabrication*, Anaheim, California, May 28-31, 2002.